Investigating Neural Dysfunction with Abnormal Protein Deposition in Alzheimer's Disease Through Magnetic Resonance Spectroscopic Imaging, Plasma Biomarkers, and Positron Emission Tomography

Kiwamu Matsuoka [1, 2*], Kosei Hirata [1], Naomi Kokubo [1], Takamasa Maeda [3], Kenji Tagai [1], Hironobu Endo [1], Keisuke Takahata [1], Hitoshi Shinotoh [1, 4], Maiko Ono [1,5], Chie Seki [1], Harutsugu Tatebe [1], Kazunori Kawamura [6], Ming-Rong Zhang [6], Hitoshi Shimada [1, 7], Takahiko Tokuda [1], Makoto Higuchi [1], Yuhei Takado [1, 5*]

[1] Department of Functional Brain Imaging, Institute for Quantum Medical Science, Quantum Life and Medical Science Directorate, National Institutes for Quantum Science and Technology, Chiba, Japan

[2] Department of Psychiatry, Nara Medical University, Nara, Japan

[3] QST Hospital, Quantum Life and Medical Science Directorate, National Institutes for Quantum Science and Technology, Chiba, Japan

[4] Neurology Clinic, Chiba, Chiba, Japan

[5] Institute for Quantum Life Science, Quantum Life and Medical Science Directorate, National Institutes for Quantum Science and Technology, Chiba, Japan

[6] Department of Advanced Nuclear Medicine Sciences, Institute for Quantum Medical Science, Quantum Life and Medical Science Directorate, National Institutes for Quantum Science and Technology, Chiba, Japan

[7] Center for integrated human brain science, Brain Research Institute, Niigata University, Niigata, Japan

***Corresponding Authors**:

Kiwamu MATSUOKA, MD, PhD

Department of Functional Brain Imaging Research, Institute for Quantum Medical Science, National Institutes for Quantum Science and Technology (QST), 4-9-1 Anagawa, Inage-ku, Chiba-shi, Chiba 263-8555, Japan

E-mail: matsuoka.kiwamu@qst.go.jp

Yuhei TAKADO, MD, PhD

Institute for Quantum Life Science, National Institutes for Quantum Science and Technology (QST), 4-9-1 Anagawa, Inage-ku, Chiba-shi, Chiba 263-8555, Japan

E-mail: takado.yuhei@qst.go.jp

Running Title: Neural Dysfunction by Abnormal Protein in AD

ABSTRACT

Background: In Alzheimer's disease (AD), aggregated abnormal proteins induce neuronal dysfunction. Despite the evidence supporting the association between tau proteins and brain atrophy, further studies are needed to explore their link to neuronal dysfunction in the human brain.

Methods: To clarify the relationship between neuronal dysfunction and abnormal proteins in AD-affected brains, we conducted magnetic resonance spectroscopic imaging (MRSI) and assessed the neurofilament light chain plasma levels (NfL). We evaluated tau and amyloid-β depositions using standardized uptake value ratios (SUVRs) of florzolotau (18F) for tau and ^{11}C-PiB for amyloid-β positron emission tomography in the same patients. Heatmaps were generated to visualize Z scores of glutamate to creatine (Glu/Cr) and N-acetylaspartate to creatine (NAA/Cr) ratios using data from healthy controls.

Results: In AD brains, Z-score maps revealed reduced Glu/Cr and NAA/Cr ratios in the gray matter, particularly in the right dorsolateral prefrontal cortex (rDLPFC) and posterior cingulate cortex (PCC). Glu/Cr ratios were negatively correlated with florzolotau (18F) SUVRs in the PCC, and plasma NfL levels were elevated and negatively correlated with Glu/Cr ($P = 0.040$, $r = -0.50$) and NAA/Cr ratios ($P = 0.003$, $r = -0.68$) in the rDLPFC.

Conclusion: This suggests that the abnormal tau proteins in AD-affected brains play a role in diminishing glutamate levels. Furthermore, neuronal dysfunction markers including Glu/tCr and NAA/tCr could potentially indicate favorable clinical outcomes. Using MRSI provided spatial information about neural dysfunction in AD, enabling the identification of vulnerabilities in the rDLPFC and PCC within the AD's pathological context.

Keywords: Alzheimer's disease, Glutamate, Magnetic resonance spectroscopy, Positron emission tomography, Neurofilament light chain plasma levels

Introduction

Alzheimer's disease (AD) is a progressive neurodegenerative disease often characterized by initial memory impairment following a cognitive decline [1]. A recent study reported the prevalence of clinical AD in the United States to be 11.3% and predicted further increases in the next four decades [2]. AD is a very burdensome disease, ranking fourth-highest in years of life lost in 2016 [3]. The neuropathologic hallmark of AD is neuronal loss paralleled by the distribution of neurofibrillary tangles composed of filamentous tau proteins and amyloid plaques [4]. The limited cognitive improvement observed upon removal of amyloid plaques with human monoclonal antibodies [5] suggests that therapeutic approaches that address other factors, including abnormal tau protein and neuronal dysfunction, may be necessary. Although the relationship between abnormal tau protein and brain atrophy has been established through previous human brain imaging studies [6], understanding the manner in which neuronal dysfunction is related to abnormal proteins *in vivo* is crucial for the development of disease-modifying treatments rooted in the fundamental pathophysiology. To the best of our knowledge, only a small number of studies have investigated this relationship in cognitively unimpaired older adults [7].

Proton magnetic resonance spectroscopy (MRS) can potentially inform us about neuronal dysfunction in diseased brains using two major metabolites, N-acetylaspartate (NAA) and glutamate (Glu). While NAA has been employed as a primary neuronal marker of viability [8], Glu measured by MRS could be a marker of metabolic activity [8] in the brain due to its relationship with glucose metabolism [9]. Studies have reported decreased Glu levels in the gray matter in patients with AD (reviewed in [10]). Furthermore, a recent meta-analysis of AD patients found reduced Glu levels in the posterior cingulate cortex (PCC), accompanied by reduced NAA levels [11]. It is speculated that Glu may be an important metabolite in AD with a potential association with tau proteins; however, it has not been examined outside of the PCC using MRS, and the mechanism by which its relationship to abnormal proteins differs from NAA is not fully understood. This non-invasive modality can be combined with

other modalities, such as positron emission tomography (PET) to evaluate brain conditions from multiple aspects.

PET imaging has enabled the evaluation of tau and amyloid-β deposition in AD pathology [12]. We reported that florzolotau (18F) (^{18}F-florzolotau) could visualize tau depositions with high contrast in patients with AD [13]. A recent study showed that tau aggregations were associated with neuronal dysfunction evaluated by NAA and Glu levels in the PCC in cognitively unimpaired older adults [7]. In the previous study, individuals with only slight abnormal protein accumulations were not excluded due to an absence cutoff of the PET standardized uptake value ratio (SUVR). On the other hand, to our knowledge, no *in vivo* imaging studies investigated the associations of NAA and Glu levels with tau aggregations in patients who developed AD.

In this study, we utilized MRS imaging (MRSI) of the cingulate gyrus of patients with AD to test our hypothesis that patients with AD exhibited decreased levels of NAA and Glu, which are indicative of neuronal viability and metabolic activity, respectively, in the PCC and its relevant brain regions. In addition, we explored the connection between these MRSI measurements and the distribution of abnormal proteins measured by PET to elucidate their relationship. Moreover, we evaluated the clinical utility of MRS metabolites by examining the association between the blood levels of neurofilament light chain (NfL), which provides a sensitive measurement of neuroaxonal damage, and the MRS metabolites (Glu and NAA).

Methods

Participants

We recruited patients with AD, including mild cognitive impairment (MCI) due to AD and AD dementia from affiliated hospitals of the National Institute of Radiological Sciences (NIRS) and National Institutes for Quantum Science and Technology (QST) between April 2019 and September 2021. All the patients

with MCI due to AD and AD dementia were diagnosed using the criteria for MCI defined by Petersen [14] and the NINCDS-ADRDA Alzheimer's Criteria as probable AD [15], respectively. We also recruited age- and sex-matched healthy controls (HCs) from the volunteer association of the NIRS-QST. All the HCs had no history of neurologic or psychiatric disorders. At the screening, all the patients with AD and HCs were confirmed to be with and without amyloid deposition, respectively, by visual assessment of PET images of ^{11}C-Pittsburgh compound-B (PiB) by three readers based on the standard method used in the Japanese Alzheimer's Disease Neuroimaging Initiative (J-ADNI) study [16]. We excluded one patient with AD and one HC because they did not complete the imaging protocol. Thirteen patients were exposed to cholinesterase inhibitors for AD (donepezil, n = 10; galantamine, n = 1; rivastigmine, n = 2). Meanwhile, we excluded one patient with AD who took memantine, a glutamate receptor antagonist. Finally, we enrolled 19 patients with AD and 27 HCs. We obtained written informed consent from all the participants and/or from spouses or other close family members when the patients were cognitively impaired. The QST Certified Review Board approved the current study.

All the participants were subjected to a series of standardized quantitative measurements of cognitive function (Mini-Mental State Examination [MMSE] [17] and Clinical Dementia Rating [CDR] [18] for AD patients) and neuropsychiatric symptoms (Apathy Scale [19] and Geriatric Depression Scale [GDS] [20]). Additionally, all HCs and some AD patients completed the Trail Making Test [TMT] [21] (18 patients for TMT-A and 15 patients for TMT-B).

MRI / MRSI data acquisition and analysis

MRI and MRSI scans were performed using a 3.0-Tesla scanner (MAGNETOM Verio; Siemens Healthcare) equipped with a 32-channel receiving head coil. Three-dimensional T1-weighted images were acquired using a magnetization-prepared rapid gradient-echo sequence (repetition time (TR) = 2,300 ms; echo time (TE) = 1.95 ms; TI = 900 ms; field of view (FOV) = 250 mm; flip angle = 9°; acquisition

matrix = 256 × 256; and axial slices of 1 mm thickness). We also performed a two-dimensional MRSI with point-resolved spectroscopy (PRESS) pulse sequence with the following parameters: TE = 30 ms, TR = 2000 ms, 3 averages, 16 × 16 chemical shift imaging matrix, and slice thickness = 15 mm. Every single volume of interest (VOI) was 10 × 10 × 15 mm^3 (FOV = 160 × 160 mm^2 including the measurement volume [mVol] = 80 × 80 × 15 mm^3). We applied 3D Shim (Syngo MR version for VD13A, Siemens, Erlangen, Germany) and subsequently performed manual shimming to reduce the linewidth of the water spectrum in magnitude mode below 25 Hz. Outer-volume suppression (OVS) [22] and water suppression were enhanced through T1 effects (WET) [23]. A trained operator placed the multivoxel VOIs at the level of the cingulate gyrus (Figure 1).

PET procedures

All the participants were examined using ^{11}C-PiB and ^{18}F-florzolotau PET. ^{11}C-PiB and ^{18}F-florzolotau were radiosynthesized by the Department of Radiopharmaceuticals Development at NIRS following our previous studies' protocols [13, 24]. The ^{18}F-florzolotau (injected dose: 185.7 ± 6.9 MBq, molar activity: 248.6 ± 76.3 GBq/μmol) PET scan was performed using Biograph mCT flow system (Siemens Healthcare). The images were reconstructed with filtered back projection. Meanwhile, the ^{11}C-PiB (injected dose: 536.1 ± 61.1 MBq, molar activity: 87.2 ± 24.6 GBq/μmol) PET scan was performed using ECAT EXACT HR+ scanner (CTI PET Systems, Inc.), Biograph mCT flow system (Siemens Healthcare), or Discovery MI (GE Healthcare). All the PET scan images were reconstructed with filtered back projection.

MRSI data analysis

We analyzed MRSI data using LCModel software (Stephen Provencher, Inc) [25] for a linear combination of model spectra provided in a basis set. We evaluated the referencing metabolite ratios of total NAA

(tNAA; NAA + N–acetyl–aspartyl–glutamate [NAAG]) and Glu to total creatine (Cr) (tCr; Cr + PCr), because tCr has been widely used as an internal reference in human studies [26]. The signal-to-noise ratio (SNR) was obtained using an NAA peak height at 2.01 ppm divided by the standard deviation (SD) of noise. For all spectra, LCModel quantification was performed on a spectral window between 0.2 and 4.2 ppm. We excluded spectra data of the most dorsal 8 voxels, based on the quality control criteria (SNR ratio < 5, full width at half maximum [FWHM] > 0.143 ppm) [27]. Additionally, data from one HC were excluded because of strong lipid contamination.

PET image processing

We applied motion correction and coregistration to the corresponding participant's T1-weighted images for PET data using PMOD® software ver. 3.8 (PMOD Technologies Ltd., Zurich, Switzerland). SUVR images were generated with cerebellar gray matter (GM) as a reference region, using ^{18}F-florzolotau PET data at 90–110-min post-injection and ^{11}C-PiB PET data at 50–70 min post-injection. For the reference region, we performed surface-based cortical reconstruction and volumetric subcortical segmentation of T1-weighted images with FreeSurfer software (version 6.0.0; http://surfer.nmr.harvard.edu). We defined regions of interest (ROIs) of the cerebellar cortex [28] (excluding the vermis [29]) as described in our previous study [30].

We defined target ROIs corresponding to the multivoxel VOIs of the measurement volume by MRSI. The multivoxel VOIs were composed 8 × 8 voxels of 80 × 80 × 15 mm^3. We manually performed coregistration of the multivoxel VOIs to the corresponding participant's T1-weighted images using screenshot images of the MRSI VOI placements as a reference (Figure S1). We evaluated ^{18}F-florzolotau and ^{11}C-PiB SUVRs in the multivoxel VOIs.

Immunoassay protocols

We measured plasma levels of the NfL from the blood samples of 26 HCs and 17 patients with AD. We applied an HD-X Simoa analyzer with reagents from a single lot using the Simoa NF-light assay, according to the protocol issued by the manufacturer (Quanterix, Lexington, MA, USA). All samples were analyzed in duplicate on one occasion.

Statistical analysis

Independent samples t-tests and χ^2-tests were used to compare baseline demographics, clinical characteristics, metabolite levels, NfL levels, and ^{18}F-florzolotau and ^{11}C-PiB SUVRs. After performing the Shapiro–Wilk test to assess whether data followed normal distribution or not, Pearson correlation (for parametric data) or Spearman's rank-order correlation (for non-parametric data) was used to evaluate the correlations between clinical characteristics, metabolite levels, NfL levels, and ^{18}F-florzolotau and ^{11}C-PiB SUVRs. All statistical tests were two-tailed, and P values of <0.05 indicated statistical significance. Statistical analyses were performed using IBM SPSS Statistics for Windows, version 25 (IBM Corp., Armonk, NY, USA).

We constructed heatmaps to visualize Z scores of ^{18}F-florzolotau and ^{11}C-PiB SUVRs and the metabolites to tCr ratios in patients with AD using data of HCs as a reference. In addition, we created a heatmap of Pearson correlation coefficients between the metabolites to tCr ratios and SUVRs of ^{18}F-florzolotau and ^{11}C-PiB SUVRs in patients with AD. We utilized GraphPad Prism version 8.4.3 (GraphPad Software) for heatmaps. Based on the results of the heatmaps, we chose VOI for further analysis to compare the metabolites with tCr ratios between patients with AD and HCs and the correlations with cognitive functions, NfL levels, and ^{18}F-florzolotau and ^{11}C-PiB SUVRs.

Results

Demographic and clinical profiles

The demographic and clinical profiles of patients with AD and HCs are summarized in Table 1. The study included eight patients with MCI and 11 with dementia. There were no statistically significant differences in age or sex between the two groups. The patients with AD showed worse cognitive functions in the total scores of MMSE and TMT-A and TMT-B than those of the HCs. There were no statistically significant differences in the symptoms of depression (GDS) or apathy (AS) between the two groups.

Heatmaps of the Z score means of ^{18}F-florzolotau and ^{11}C-PiB SUVRs

All the patients with AD demonstrated typical depositions of ^{18}F-florzolotau in the neocortical and limbic cortices, in line with our previous study [13] (Figure 2a). They also showed ^{11}C-PiB depositions in the cortices corresponding to the J-ADNI study criteria [16] (Figure 2b). The heatmaps of the Z score means of ^{18}F-florzolotau and ^{11}C-PiB SUVRs were markedly increased in the neocortical and limbic cortices (Figure 2c, d).

Heatmaps of Glu/tCr and tNAA/tCr ratios

The heatmap showed decreased Z scores of Glu/tCr ratios in the GM, especially in the PCC and right dorsolateral prefrontal cortex (rDLPFC) (Figure 3a). The heatmap also demonstrated decreases in tNAA/tCr ratios in the GM, including the PCC and rDLPFC (Figure 3b).

The heatmaps of Pearson correlation coefficients of ^{18}F-florzolotau and ^{11}C-PiB SUVRs showed a marked negative correlation of Glu/tCr ratios with ^{18}F-florzolotau SUVR in the PCC regions (Figure 3c–f).

Glu/tCr and tNAA/tCr ratios in the PCC and rDLPFC and their correlations with ^{18}F-florzolotau and ^{11}C-PiB SUVRs and cognitive batteries

Given that the heatmaps indicated decreased Glu/tCr and tNAA/tCr ratios in the PCC and rDLPFC, we

subsequently analyzed the coalesced voxels covering the PCC and rDLPFC (Figure S2). We found that Glu/tCr and tNAA/tCr ratios were both significantly decreased in the PCC and rDLPFC in patients with AD compared with that of the HCs (Glu/tCr ratios, $P < 0.05$ in the PCC and $P < 0.005$ in the rDLPFC; tNAA/tCr ratios, $P < 0.05$ in the PCC and $P < 0.001$ in the rDLPFC) (Figure 4). We also found a correlation between tNAA/tCr ratios in the PCC and rDLPFC ($r = 0.52$, $P = 0.023$), but not with Glu/tCr ($r = 0.16$, $P = 0.51$).

The heatmap revealed a negative correlation of ^{18}F-florzolotau SUVRs with Glu/tCr ratios in the PCC but with not tNAA (Glu/tCr ratios, $P = 0.046$ and $r = -0.46$; tNAA/tCr ratios, $P = 0.62$ and $r = 0.12$) (Figure 5a-b). There was no significant correlation with ^{11}C-PiB SUVRs in the PCC (Glu/tCr ratios, $P = 0.53$ and $r = -0.15$; tNAA/tCr ratios, $P = 0.11$ and $r = 0.38$) (Figure 5c-d). We observed no significant correlation with SUVRs of ^{18}F-florzolotau and ^{11}C-PiB in the rDLPFC (Glu/tCr ratios, $P = 0.64$ and $r = -0.12$; tNAA/tCr ratios, $P = 0.19$ and $r = -0.32$ for ^{18}F-florzolotau; Glu/tCr ratios, $P = 0.46$ and $r = -0.18$; tNAA/tCr ratios, $P = 0.17$ and $r = -0.33$ for ^{11}C-PiB).

In the rDLPFC, Glu/tCr and tNAA/tCr ratios were positively correlated with the MMSE total scores in patients with AD (Glu/tCr ratios, $P < 0.001$ and $r = 0.72$; tNAA/tCr ratios, $P < 0.001$ and $r = 0.75$) (Figure 6a, b); the Glu/tCr and tNAA/tCr ratios in the PCC were not correlated with the MMSE total scores (Glu/tCr ratios, $P = 0.15$ and $r = 0.35$; tNAA/tCr ratios, $P = 0.14$ and $r = 0.35$) (Table S1). In patients with AD, we also found negative correlations between Glu/tCr ratios in the PCC and TMT-A time and between tNAA/tCr ratios in the rDLPFC and TMT-B time (Glu/tCr ratios, $P = 0.002$ and $r = -0.68$; tNAA/tCr ratios, $P = 0.53$ and $r = -0.16$ in the PCC; Glu/tCr ratios, $P = 0.22$ and $r = -0.31$; tNAA/tCr ratios, $P = 0.050$ and $r = -0.47$ in the rDLPFC for TMT-A; Glu/tCr ratios, $P = 0.83$ and $r = -0.061$; tNAA/tCr ratios, $P = 0.55$ and $r = 0.17$ in the PCC; Glu/tCr ratios, $P = 0.95$ and $r = 0.017$; tNAA/tCr ratios, $P = 0.007$ and $r = -0.66$ in the rDLPFC for TMT-B) (Figure 6c, d and Table S1).

Correlations of Glu/tCr and tNAA/tCr ratios in the PCC and rDLPFC with blood NfL levels

We found higher NfL levels in the blood in patients with AD than that in the HCs ($P < 0.005$) (Figure 7a). We found negative correlations between blood NfL levels and Glu/tCr ratios ($P = 0.040$ and $r = -0.50$) and tNAA/tCr ratios ($P = 0.003$ and $r = -0.68$) in the rDLPFC. There were also trends of negative correlations between blood NfL levels and Glu/tCr ratios ($P = 0.10$ and $r = -0.41$) or tNAA/tCr ratios ($P = 0.086$ and $r = -0.43$) in the PCC, although these correlations did not reach a statistical significance level (Figure 7b–e).

Discussion

The MRSI technique revealed decreases in Glu/tCr and tNAA/tCr ratios in the PCC and rDLPFC, which were associated with impaired cognitive functions in patients with AD. Glu/tCr ratios, rather than tNAA/tCr ratios, exhibited a negative correlation with the levels of tau depositions in the PCC. Moreover, Glu/tCr and tNAA/tCr ratios in the rDLPFC were negatively associated with NfL levels, which provide a sensitive measurement of neuroaxonal damage.

The Glu/tCr and tNAA/tCr ratios in the PCC were lower in patients with AD compared with that of the HCs. While only the Glu/tCr ratio was found to correlate with ^{18}F-florzolotau SUVRs in the PCC, the lack of correlation with the tNAA/tCr ratios requires further investigation. Glu is an essential metabolic biomarker, as previous research indicates that more than 50% of glucose eventually metabolizes to glutamate in the brain [9]. Recent meta-analysis studies have linked reduced brain glucose metabolism, mitochondrial dysfunction, and oxidative stress to pathology in AD, which induces synaptic damage and neuronal death [31, 32]. In a previous study, the observed correlation between tau accumulation levels and Glu levels in the PCC of cognitively unimpaired patients is consistent with our findings [7]. Tau pathology might reflect the alteration in neuronal functions compared with amyloid pathology, which reaches saturation in the early AD stage [1]. Future preclinical studies could use a

tauopathy mouse model to investigate the role of impaired brain glucose metabolism and mitochondrial function to elucidate the underlying mechanism of the relationship between decreased Glu levels and tau depositions. Furthermore, longitudinal studies in human and tau mouse models may clarify the time series of these associations.

In an exploratory MRSI study, reduced Glu/tCr and tNAA/tCr ratios were observed not only in the PCC but also in the rDLPFC, indicating the potential for the latter region to be a useful assessment region for MRS [33, 34]. Prior studies on Glu levels in the DLPFC of patients with AD have reported inconsistent results, potentially due to the evaluation of Glx (Glu + glutamine [Gln]) rather than Glu alone. However, our measurement of Glu levels independent from Gln levels revealed reduced Glu levels in the rDLPFC of patients with dementia due to MCI and AD. Differences in AD and HC were observed in the rDLPFC but not in the left dominant hemisphere. While this study only captured changes in the rDLPFC, the differences between the left and rDLPFC in patients with AD patients remain unclear. The results of a previous study utilizing ^{18}F-FDG PET were in agreement with our investigations, indicating a decrease in metabolism of the DLPFC in the early stages of AD [35], particularly in the right hemisphere [36]. Nevertheless, MRSI is not without limitations, because chemical shift displacement may introduce ambiguity when interpreting interhemispheric discrepancies. Therefore, validation of the left–right difference of DLPFC function in AD should be further pursued using advanced MRS techniques, such as sLASER [37], which exhibits lower chemical shift displacement.

Conversely, our findings in the rDLPFC revealed positive associations between the Glu/tCr and tNAA/tCr ratios and the overall MMSE scores, while the tNAA/tCr ratio demonstrated an inverse correlation with TMT-B completion time. These results indicate that the outcomes in the rDLPFC are not a happenstance, but rather hold potential as a valuable appraisal domain for MRS, akin to the PCC. Given that the DLPFC has been shown to play a critical role in visual working memory [38, 39], it is plausible that reduced metabolic activity and neuronal survival in patients with AD may be linked to compromised

working memory function.

Both MRSI and blood biomarkers showed neural dysfunctions in patients with AD, and as an alternative to PET, blood biomarkers and MRSI measurements are less invasive and less costly, making them potentially appropriate for use in primary care. Blood biomarkers, in particular, require less testing time. NfL has been established as a biomarker of neural damage in various neurological diseases, including AD, based on accumulating evidence [40]. MRSI is a non-invasive technique that provides spatial information on metabolite levels in the brain without requiring additional imaging modalities. However, the practical application of MRSI may be limited by the technical expertise required for imaging and data analysis. In this study, a single-slice MRSI approach was used to cover a portion of the brain region of interest, but recent technological advancements have enabled 3D imaging. Although resting-state functional MRI has been extensively utilized to assess the functional network of brain diseases, MRSI can directly evaluate neural viability and metabolic activity, and thus may provide useful complementary information for future brain network assessment from a different perspective.

The present study had a limitation. We acquired ^{11}C-PiB PET data using three scanners, and our ^{11}C-PiB PET results should be interpreted with caution while considering the effects of different scanners [41, 42].

Conclusions

The MRSI technique revealed neural dysfunctions, including metabolic activity, linked with tau aggregations in the PCC. MRSI has the potential to provide spatial information regarding neural functions, leading to our findings of deteriorated neural viability and metabolic activity in the rDLPFC of patients with AD. MRSI could qualify metabolic levels in several brain regions simultaneously. The robustness of MRSI data was demonstrated by its relationship with NfL, which is commonly used in blood biomarker studies. Together with resting-state functional MRI, these MRSI measurements may have the potential to

elucidate brain network impairments.

Acknowledgements

The authors thank all patients and their caregivers for participation in this study, clinical research coordinators, PET and MRI operators, animal care technicians, radiochemists, and research ethics advisers at QST for their assistance in the current projects. We thank APRINOIA Therapeutics for kindly sharing the precursor of ^{18}F-florzolotau. The authors acknowledge support for the recruitment of patients by Dr. Shigeki Hirano at the Chiba University and Dr. Yasumasa Yoshiyama, at Inage Neurology and Memory Clinic.

Financial Support This work was supported in part by AMED [grant numbers JP19dm0207072, JP 22dk0207055, and JP22dk0207063] and JSPS KAKENHI [grant numbers JP19H01041, JP16H05324, and JP20K16681].

Conflicts of Interest H.S. (Hitoshi Shimada), M.-R.Z., T.S., and M.H. hold patents on compounds related to the present report (JP 5422782/EP 12 884 742.3/CA2894994/HK1208672). All other authors report no biomedical financial interests or potential conflicts of interest.

Supplementary Material

For supplementary material accompanying this paper, visit cambridge.org/EPA.

Author Contributions

Conceived and designed the study: K.M., Y.T. Supervised the project: M.-R.Z., T.T., M.H. Performed scans and tests: K.M., K.H., N.K., T.M., K.T. (Kenji Tagai), H.E., K.T. (Keisuke Takahata), H.S. (Hitoshi

Shinotoh), and K.K., H.S. (Hitoshi Shimada). Analyzed MRS data: K.M., K.H., T.M., Y.T. Analyzed PET data: K.M., K.H., K.T. (Kenji Tagai), H.E., C.S. Analyzed biomarker data: K.T. (Kenji Tagai), H.T., T.T., Performed statistical analysis: K.M., Y.T. Interpreted the data: K.M., K.H., N.K., T.M., K.T. (Kenji Tagai), H.E., K.T. (Keisuke Takahata), H.S. (Hitoshi Shinotoh), M.O., C.S., H.T., K.K., M.-R.Z., H.S. (Hitoshi Shimada), T.T., M.H., Y.T., Wrote the first draft: K.M., Y.T. Reviewed manuscript: K.M., K.H., N.K., T.M., K.T. (Kenji Tagai), H.E., K.T. (Keisuke Takahata), H.S. (Hitoshi Shinotoh), M.O., C.S., H.T., K.K., M.-R.Z., H.S. (Hitoshi Shimada), T.T., M.H., Y.T., K.M., and Y.T. are responsible for the overall content as a guarantor.

References

[1] Jack CR Jr, Knopman DS, Jagust WJ, Petersen RC, Weiner MW, Aisen PS, et al. Tracking pathophysiological processes in Alzheimer's disease: an updated hypothetical model of dynamic biomarkers. Lancet Neurol. 2013;12: 207-216. https://doi.org/10.1016/S1474-4422(12)70291-0.

[2] Rajan KB, Weuve J, Barnes LL, McAninch EA, Wilson RS, Evans DA. Population estimate of people with clinical Alzheimer's disease and mild cognitive impairment in the United States (2020-2060). Alzheimers Dement. 2021;17: 1966-1975. https://doi.org/10.1002/alz.12362.

[3] US Burden of Disease Collaborators, Mokdad AH, Ballestros K, Echko M, Glenn S, Olsen HE, Mullany E, et al. The state of US health, 1990-2016: burden of diseases, injuries, and risk factors among US states. JAMA. 2018;319: 1444-1472. https://doi.org/10.1001/jama.2018.0158.

[4] DeTure MA, Dickson DW. The neuropathological diagnosis of Alzheimer's disease. Mol Neurodegener. 2019;14: 32. https://doi.org/10.1186/s13024-019-0333-5.

[5] van Dyck CH, Swanson CJ, Aisen P, Bateman RJ, Chen C, Gee M, et al. Lecanemab in early Alzheimer's disease. N Engl J Med. 2023;388: 9-21. https://doi.org/10.1056/NEJMoa2212948.

[6] Shimada H, Kitamura S, Shinotoh H, Endo H, Niwa F, Hirano S, et al. Association between Aβ and tau accumulations and their influence on clinical features in aging and Alzheimer's disease spectrum brains: A [(11)C]PBB3-PET study. Alzheimers Dement (Amst). 2017;6: 11-20. https://doi.org/10.1016/j.dadm.2016.12.009.

[7] Kara F, Joers JM, Deelchand DK, Park YW, Przybelski SA, Lesnick TG, et al.. 1H MR spectroscopy biomarkers of neuronal and synaptic function are associated with tau deposition in cognitively unimpaired older adults. Neurobiol Aging. 2022;112: 16-26. https://doi.org/10.1016/j.neurobiolaging.2021.12.010.

[8] Rae CD. A guide to the metabolic pathways and function of metabolites observed in human brain 1H magnetic resonance spectra. Neurochem Res. 2014;39: 1-36.

https://doi.org/10.1007/s11064-013-1199-5.

[9] Sugiura Y, Honda K, Kajimura M, Suematsu M. Visualization and quantification of cerebral metabolic fluxes of glucose in awake mice. Proteomics. 2014;14(7-8): 829-838. https://doi.org/10.1002/pmic.201300047.

[10] Graff-Radford J, Kantarci K. Magnetic resonance spectroscopy in Alzheimer's disease. Neuropsychiatr Dis Treat. 2013;9: 687-696. https://doi.org/10.2147/NDT.S35440.

[11] Liu H, Zhang D, Lin H, Zhang Q, Zheng L, Zheng Y, et al. Meta-analysis of neurochemical changes estimated via magnetic resonance spectroscopy in mild cognitive impairment and Alzheimer's disease. Front Aging Neurosci. 2021;13: 738971. https://doi.org/10.3389/fnagi.2021.738971.

[12] Maschio C, Ni R. Amyloid and tau positron emission tomography imaging in Alzheimer's disease and other tauopathies. Front Aging Neurosci. 2022;14: 838034. https://doi.org/10.3389/fnagi.2022.838034.

[13] Tagai K, Ono M, Kubota M, Kitamura S, Takahata K, Seki C, et al. High-contrast in vivo imaging of tau pathologies in Alzheimer's and non-Alzheimer's disease tauopathies. Neuron. 2021;109: 42-58.e8. https://doi.org/10.1016/j.neuron.2020.09.042.

[14] Petersen RC, Smith GE, Waring SC, Ivnik RJ, Tangalos EG, Kokmen E. Mild cognitive impairment: clinical characterization and outcome. Arch Neurol. 1999;56: 303-308. https://doi.org/10.1001/archneur.56.3.303.

[15] McKhann G, Drachman D, Folstein M, Katzman R, Price D, Stadlan EM. Clinical diagnosis of Alzheimer's disease: report of the NINCDS-ADRDA Work Group under the auspices of Department of Health and Human Services Task Force on Alzheimer's Disease. Neurology. 1984;34: 939-944. https://doi.org/10.1212/wnl.34.7.939.

[16] Yamane T, Ishii K, Sakata M, Ikari Y, Nishio T, Ishii K, et al. Inter-rater variability of visual

interpretation and comparison with quantitative evaluation of (11)C-PiB PET amyloid images of the Japanese Alzheimer's Disease Neuroimaging Initiative (J-ADNI) multicenter study. Eur J Nucl Med Mol Imaging. 2017;44: 850-857. https://doi.org/10.1007/s00259-016-3591-2.

[17] Folstein MF, Folstein SE, McHugh PR. 'Mini-mental state'. A practical method for grading the cognitive state of patients for the clinician. J Psychiatr Res. 1975;12: 189-198. https://doi.org/10.1016/0022-3956(75)90026-6.

[18] Morris JC. Clinical dementia rating: a reliable and valid diagnostic and staging measure for dementia of the Alzheimer type. Int Psychogeriatr. 1997;9(suppl 1): 173-176; discussion 7-8. https://doi.org/10.1017/s1041610297004870.

[19] Starkstein SE, Fedoroff JP, Price TR, Leiguarda R, Robinson RG. Apathy following cerebrovascular lesions. Stroke. 1993;24: 1625-1630. https://doi.org/10.1161/01.str.24.11.1625.

[20] Lesher EL, Berryhill JS. Validation of the Geriatric Depression Scale—Short Form among inpatients. J Clin Psychol. 1994;50: 256-260. https://doi.org/10.1002/1097-4679(199403)50: 2<256: : aid-jclp2270500218>3.0.co;2-e.

[21] Tombaugh TN. Trail Making Test A and B: normative data stratified by age and education. Arch Clin Neuropsychol Off J Natl Acad Neuropsychol. 2004;19: 203-214. https://doi.org/10.1016/S0887-6177(03)00039-8.

[22] Tkác I, Andersen P, Adriany G, Merkle H, Ugurbil K, Gruetter R. In vivo 1H NMR spectroscopy of the human brain at 7 T. Magn Reson Med. 2001;46: 451-456. https://doi.org/10.1002/mrm.1213.

[23] Ogg RJ, Kingsley PB, Taylor JS. WET, a T1- and B1-insensitive water-suppression method for in vivo localized 1H NMR spectroscopy. J Magn Reson B. 1994;104: 1-10. https://doi.org/10.1006/jmrb.1994.1048.

[24] Maruyama M, Shimada H, Suhara T, Shinotoh H, Ji B, Maeda J, et al. Imaging of tau pathology

in a tauopathy mouse model and in Alzheimer patients compared to normal controls. Neuron. 2013;79: 1094-1108. https://doi.org/10.1016/j.neuron.2013.07.037.

[25] Provencher SW. Estimation of metabolite concentrations from localized in vivo proton NMR spectra. Magn Reson Med. 1993;30: 672-679. https://doi.org/10.1002/mrm.1910300604.

[26] Wilson M, Andronesi O, Barker PB, Bartha R, Bizzi A, Bolan PJ, et al. Methodological consensus on clinical proton MRS of the brain: review and recommendations. Magn Reson Med. 2019;82: 527-550. https://doi.org/10.1002/mrm.27742.

[27] Zhou M, Zhou Y, Liao H, Rowland BC, Kong X, Arvold ND, et al. Diagnostic accuracy of 2-hydroxyglutarate magnetic resonance spectroscopy in newly diagnosed brain mass and suspected recurrent gliomas. Neuro-Oncology. 2018;20: 1262-1271. https://doi.org/10.1093/neuonc/noy022.

[28] Fischl B, Salat DH, Busa E, Albert M, Dieterich M, Haselgrove C, et al. Whole brain segmentation: automated labeling of neuroanatomical structures in the human brain. Neuron. 2002;33: 341-355. https://doi.org/10.1016/s0896-6273(02)00569-x.

[29] Greve DN, Salat DH, Bowen SL, Izquierdo-Garcia D, Schultz AP, Catana C, et al.. Different partial volume correction methods lead to different conclusions: an (18)F-FDG-PET study of aging. Neuroimage. 2016;132: 334-343. https://doi.org/10.1016/j.neuroimage.2016.02.042.

[30] Matsuoka K, Takado Y, Tagai K, Kubota M, Sano Y, Takahata K, et al. Two pathways differentially linking tau depositions, oxidative stress, and neuronal loss to apathetic phenotypes in progressive supranuclear palsy. J Neurol Sci. 2023;444: 120514. https://doi.org/10.1016/j.jns.2022.120514.

[31] Ma HR, Sheng LQ, Pan PL, Wang GD, Luo R, Shi HC, et al. Cerebral glucose metabolic prediction from amnestic mild cognitive impairment to Alzheimer's dementia: a meta-analysis. Transl Neurodegener. 2018;7: 9. https://doi.org/10.1186/s40035-018-0114-z.

[32] Song T, Song X, Zhu C, Patrick R, Skurla M, Santangelo I, et al. Mitochondrial dysfunction, oxidative stress, neuroinflammation, and metabolic alterations in the progression of Alzheimer's disease: A meta-analysis of in vivo magnetic resonance spectroscopy studies. Ageing Res Rev. 2021;72: 101503. https://doi.org/10.1016/j.arr.2021.101503.

[33] Gozdas E, Hinkley L, Fingerhut H, Dacorro L, Gu M, Sacchet MD, et al. 1H-MRS neurometabolites and associations with neurite microstructures and cognitive functions in amnestic mild cognitive impairment. NeuroImage Clin. 2022;36: 103159. https://doi.org/10.1016/j.nicl.2022.103159.

[34] Tumati S, Opmeer EM, Marsman JC, Martens S, Reesink FE, De Deyn PP, et al. Lower choline and myo-inositol in temporo-parietal cortex is associated with apathy in amnestic MCI. Front Aging Neurosci. 2018;10: 106. https://doi.org/10.3389/fnagi.2018.00106.

[35] Strom A, Iaccarino L, Edwards L, Lesman-Segev OH, Soleimani-Meigooni DN, Pham J, et al. Cortical hypometabolism reflects local atrophy and tau pathology in symptomatic Alzheimer's disease. Brain. 2022;145: 713-728. https://doi.org/10.1093/brain/awab294.

[36] Riederer I, Bohn KP, Preibisch C, Wiedemann E, Zimmer C, Alexopoulos P, et al. Alzheimer disease and mild cognitive impairment: integrated pulsed arterial spin-labeling MRI and (18)F-FDG PET. Radiology. 2018;288: 198-206. https://doi.org/10.1148/radiol.2018170575.

[37] Pradhan S, Bonekamp S, Gillen JS, Rowland LM, Wijtenburg SA, Edden RA, et al. Comparison of single voxel brain MRS AT 3T and 7T using 32-channel head coils. Magn Reson Imaging. 2015;33: 1013-1018. https://doi.org/10.1016/j.mri.2015.06.003.

[38] Li S, Cai Y, Liu J, Li D, Feng Z, Chen C, et al. Dissociated roles of the parietal and frontal cortices in the scope and control of attention during visual working memory. Neuroimage. 2017;149: 210-219. https://doi.org/10.1016/j.neuroimage.2017.01.061.

[39] Owen AM, McMillan KM, Laird AR, Bullmore E. N-back working memory paradigm: a

meta-analysis of normative functional neuroimaging studies. Hum Brain Mapp. 2005;25: 46-59. https://doi.org/10.1002/hbm.20131.

[40] Khalil M, Teunissen CE, Otto M, Piehl F, Sormani MP, Gattringer T, et al. Neurofilaments as biomarkers in neurological disorders. Nat Rev Neurol. 2018;14: 577-589. https://doi.org/10.1038/s41582-018-0058-z.

[41] Albano D, Gatta R, Marini M, Rodella C, Camoni L, Dondi F, et al. Role of 18F-FDG PET/CT Radiomics Features in the Differential Diagnosis of Solitary Pulmonary Nodules: Diagnostic Accuracy and Comparison between Two Different PET/CT Scanners. J Clin Med. 2021;18. https://doi.org/10.3390/jcm10215064.

[42] Dondi F, Pasinetti N, Gatta R, Albano D, Giubbini R, Bertagna F. Comparison between two different scanners for the evaluation of the role of 18F-FDG PET/CT Semiquantitative Parameters and Radiomics Features in the Prediction of Final Diagnosis of Thyroid Incidentalomas. J Clin Med. 2022(3);18(3). https://doi.org/10.3390/jcm11030615.

Data Availability

The datasets generated during and/or analyzed during the current study are available from the corresponding author on reasonable request.

Ethics approval

This study was approved by the Institutional Review Board of the NIRS. Written informed consent was obtained from all patients and from their spouses or other close family members. The study was registered with the UMIN clinical Trials Registry (UMIN-CTR; number 000030248).

Consent to participate

Informed consent was obtained from all individual participants included in the study." OR "Written informed consent was obtained from the parents.

Consent to publish

Obtained.

Figure Legends

Fig. 1 Multiple voxels of interest VOIs and representative spectrum of MRSI

a) We placed the multivoxel VOIs at the level of the cingulate gyrus. We obtained usable spectra from the $10 \times 10 \times 15$ mm^3 voxels (green squares) within the PRESS excitation volume (white box). b) An example of spectral data, spectral fit, fit residual, baseline, and individual metabolite fits obtained from the voxel (blue voxel).

Glu, glutamate; NAA, N-acetylaspartate; NAA, N-acetylaspartate; NAAG, N–acetyl–aspartyl–glutamate; MRSI, magnetic resonance spectrum imaging; PRESS, point-resolved spectroscopy; VOI, volume of interest

Fig. 2 Representative PET SUVR images of a patient with AD and heatmaps of Z score means of ^{18}F-florzolotau and ^{11}C-PiB

a, b) A representative PET image of ^{18}F-florzolotau (left) and ^{11}C-PiB (right) in patients with AD showed accumulations in the neocortical and limbic cortices. c, d) Z-score heatmaps of ^{18}F-florzolotau (left) and ^{11}C-PiB (right) in patients with AD also indicated marked increases in the neocortical and limbic cortices.

AD, Alzheimer's disease; PET, positron emission tomography; PiB, Pittsburgh compound-B; SUVR, standardized uptake value ratios

Fig. 3 Heatmaps of Z score means of Glu/tCr and tNAA/tCr ratios and heatmaps of Pearson correlation coefficients with ^{18}F-florzolotau and ^{11}C-PiB SUVRs

a, b) The heatmap showed decreased Z scores of Glu (upper) and tNAA (lower) to tCr ratio in the GM, especially in the PCC and rDLPFC in patients with AD. c, d) The heatmaps of Pearson correlation coefficients displayed a marked negative correlation of Glu/tCr ratios with ^{18}F-florzolotau SUVR in the PCC regions (upper), not but with ^{11}C-PiB (lower) in patients with AD. e, f) The heatmaps of Pearson

correlation coefficients indicated no extensive areas where ^{11}C-PiB SUVRs were correlated with Glu (upper) and (lower) to the tCr ratio in patients with AD. Stars indicate that the absolute value of Pearson correlation coefficients is greater than 0.5.

AD, Alzheimer's disease; Cr, creatine; rDLPFC, right dorsolateral prefrontal cortex; Glu, glutamate; GM, gray matter; NAA, N-acetylaspartate; PCC, posterior cingulate cortex; PET, positron emission tomography; PiB, Pittsburgh compound-B; SUVR, standardized uptake value ratios

Fig. 4 Scatterplots showing differences in the Glu/tCr and tNAA/tCr ratios between the patients with AD and HCs

Both the Glu/tCr and tNAA/tCr ratios were significantly decreased in the PCC and rDLPFC in patients with AD compared with those in the HCs (right upper, Glu/tCr ratios in the PCC; left upper, Glu/tCr ratios in the rDLPFC; right lower, tNAA/tCr ratios in the PCC; left lower, tNAA/tCr ratios in the rDLPFC).

AD, Alzheimer's disease; Cr, creatine; rDLPFC, right dorsolateral prefrontal cortex; Glu, glutamate; HC, healthy control; NAA, N-acetylaspartate; PCC, posterior cingulate cortex; PET, positron emission tomography; PiB, Pittsburgh compound-B. * P values are <0.05, *** P values are <0.005, **** P values are <0.001

Fig. 5 Scatterplot showing correlations of Glu/tCr and tNAA/tCr ratios with ^{18}F-florzolotau and ^{11}C-PiB SUVR in patients with AD

We found a negative correlation between ^{18}F-florzolotau SUVRs and Glu/tCr ratios (upper left) in the PCC, but not with tNAA (upper right). There was no correlation of ^{11}C-PiB SUVRs with Glu/tCr ratios (lower left) nor tNAA (lower right). AD, Alzheimer's disease; Cr, creatine; Glu, glutamate; NAA, N-acetylaspartate; PCC, posterior cingulate cortex; SUVR, standardized uptake value ratios.

Fig. 6 Scatterplot showing correlations of Glu/tCr and tNAA/tCr ratios with cognitive batteries in patients with AD

a, b) The Glu (upper left) and tNAA/tCr ratios (upper right) in the rDLPFC were positively correlated with MMSE total scores in patients with AD. c, d) We also found a negative correlations between Glu/tCr ratios in the PCC and TMT-A time (lower left) and between tNAA/tCr ratios in the rDLPFC and TMT-B time (lower right) in patients with AD.

AD, Alzheimer's disease; Cr, creatine; rDLPFC, right dorsolateral prefrontal cortex; Glu, glutamate; NAA, N-acetylaspartate; PCC, posterior cingulate cortex

Fig. 7 Scatterplots showing the comparison of blood NfL levels and the correlations of Glu/tCr and tNAA/tCr ratios with blood NfL levels in patients with AD

a) We found higher NfL levels in the blood of patients with AD than that in HCs. b-e) We found significant negative correlations between blood NfL levels and Glu/tCr ratios (upper right) and tNAA/tCr ratios (lower right) in the rDLPFC. There were also negative correlations between blood NfL levels and Glu/tCr ratios (upper left) and tNAA/tCr ratios (lower left) in the PCC, although these correlations did not reach a statistical significance level.

AD, Alzheimer's disease; Cr, creatine; rDLPFC, right dorsolateral prefrontal cortex; Glu, glutamate; NAA, N-acetylaspartate; NfL, neurofilament light chain; PCC, posterior cingulate cortex. *** P values are <0.005

a)

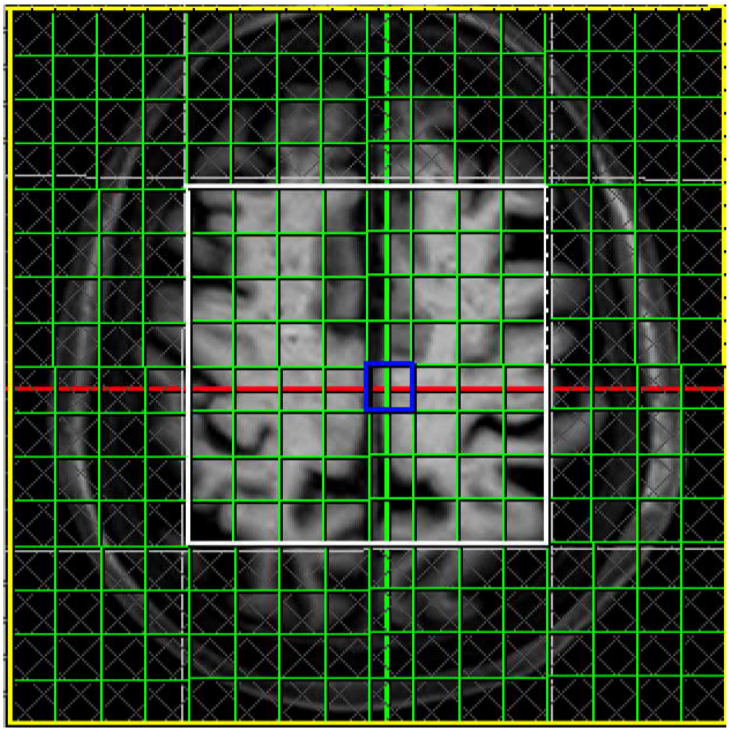

b)

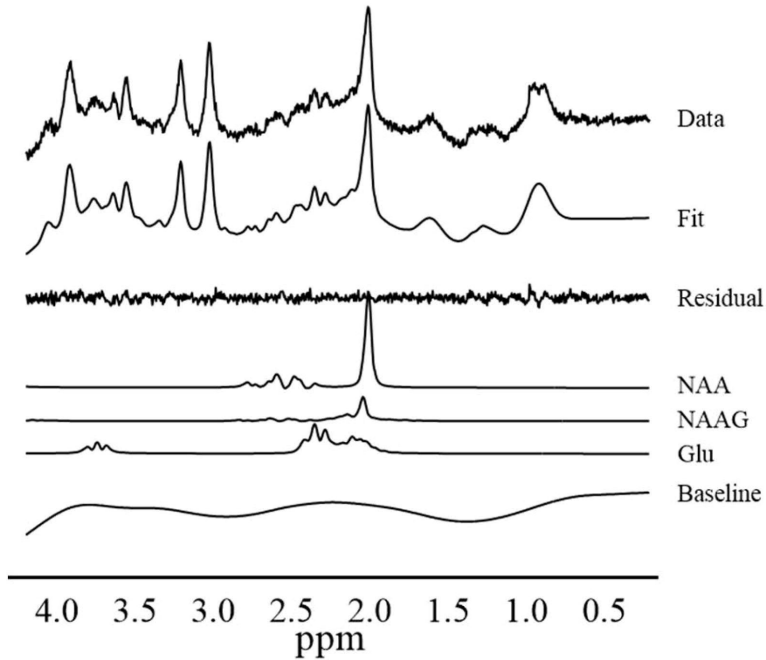
Data
Fit
Residual
NAA
NAAG
Glu
Baseline
4.0
3.5
3.0
2.5
2.0
1.5
1.0
0.5
ppm

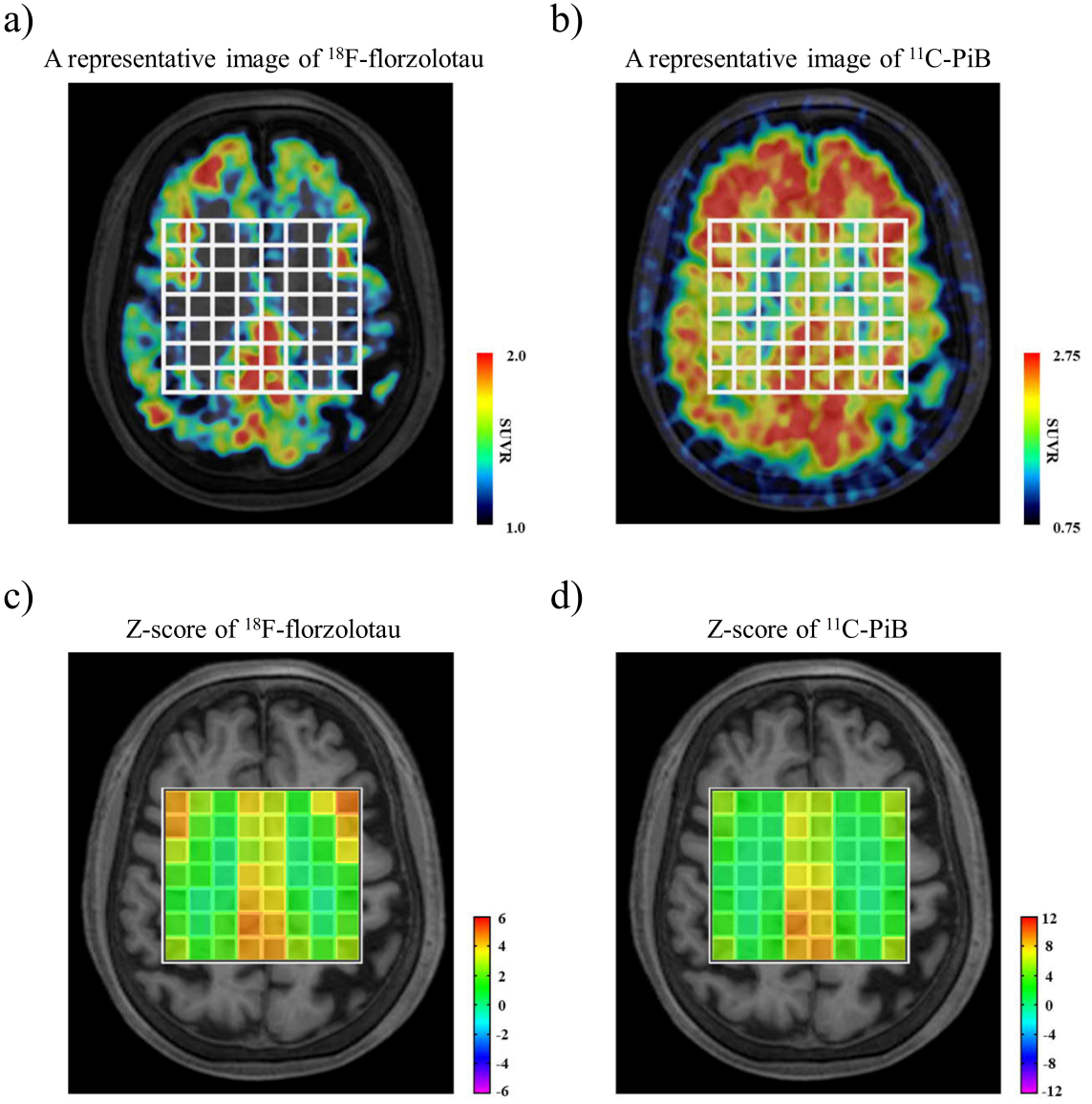
a)
A representative image of 18F-florzolotau
2.0
SUVR
1.0
b)
A representative image of 11C-PiB
2.75
SUVR
0.75
c)
Z-score of 18F-florzolotau
6
4
2
0
-2
-4
-6
d)
Z-score of 11C-PiB
12
8
4
0
-4
-8
-12

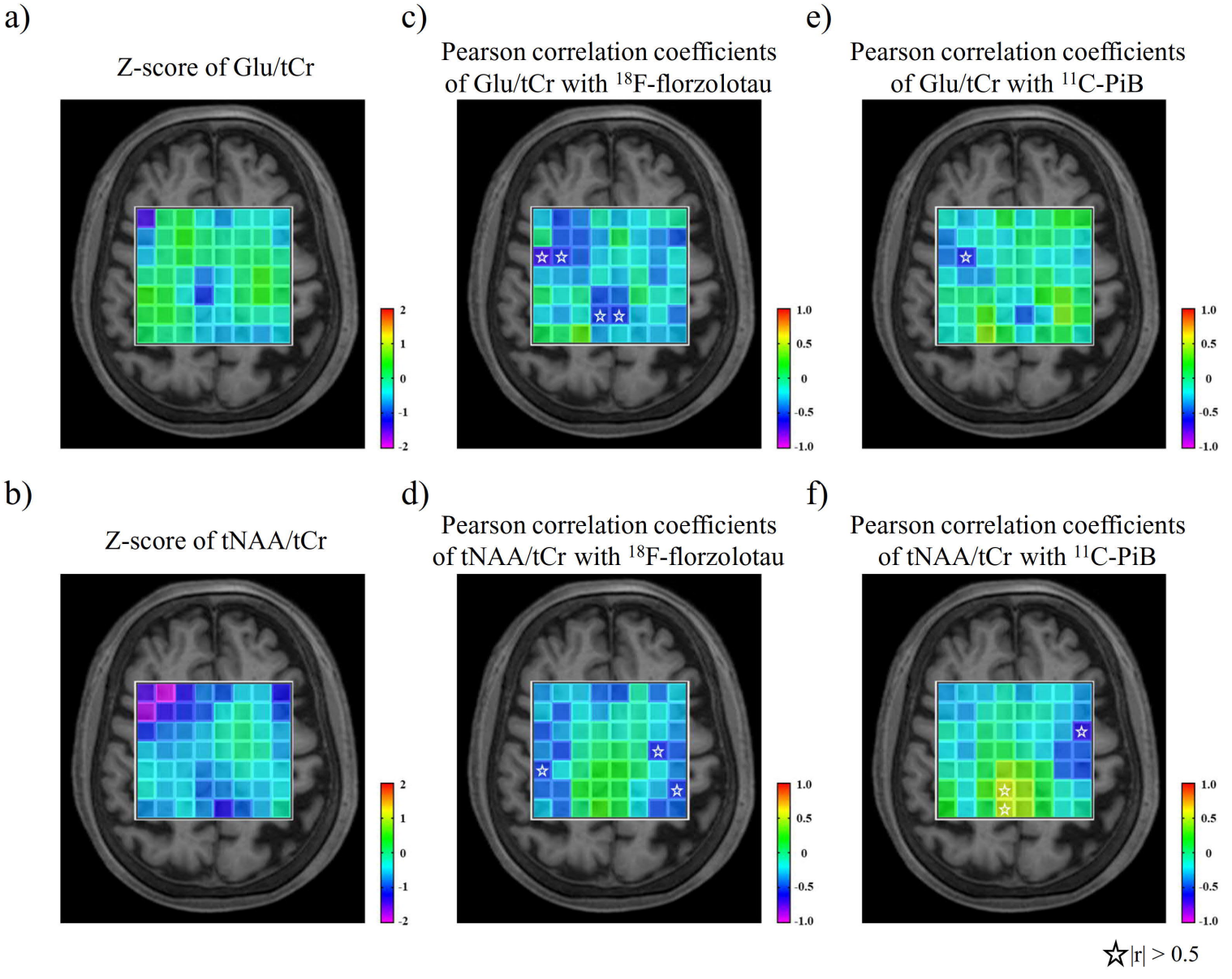
a)
Z-score of Glu/tCr
2
1
0
-1
-2
b)
Z-score of tNAA/tCr
2
1
0
-1
-2
c)
Pearson correlation coefficients of Glu/tCr with 18F-florzolotau
1.0
0.5
0
-0.5
-1.0
d)
Pearson correlation coefficients of tNAA/tCr with 18F-florzolotau
1.0
0.5
0
-0.5
-1.0
e)
Pearson correlation coefficients of Glu/tCr with 11C-PiB
1.0
0.5
0
-0.5
-1.0
f)
Pearson correlation coefficients of tNAA/tCr with 11C-PiB
1.0
0.5
0
-0.5
-1.0
☆|r| > 0.5

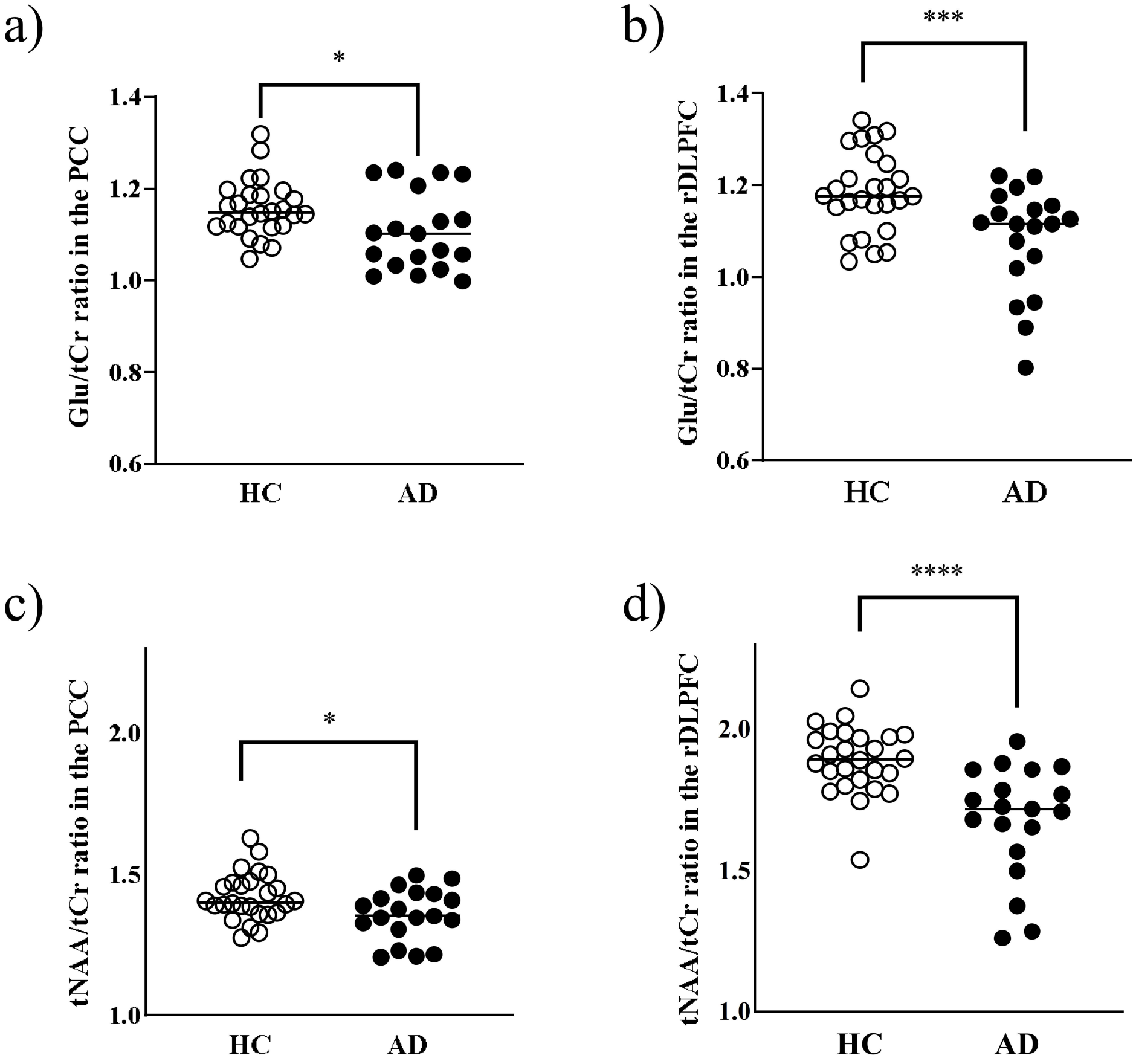
a)
*
Glu/tCr ratio in the PCC
1.4
1.2
1.0
0.8
0.6
HC
AD
b)
***
Glu/tCr ratio in the rDLPFC
1.4
1.2
1.0
0.8
0.6
HC
AD
c)
*
tNAA/tCr ratio in the PCC
2.0
1.5
1.0
HC
AD
d)
****
tNAA/tCr ratio in the rDLPFC
2.0
1.5
1.0
HC
AD

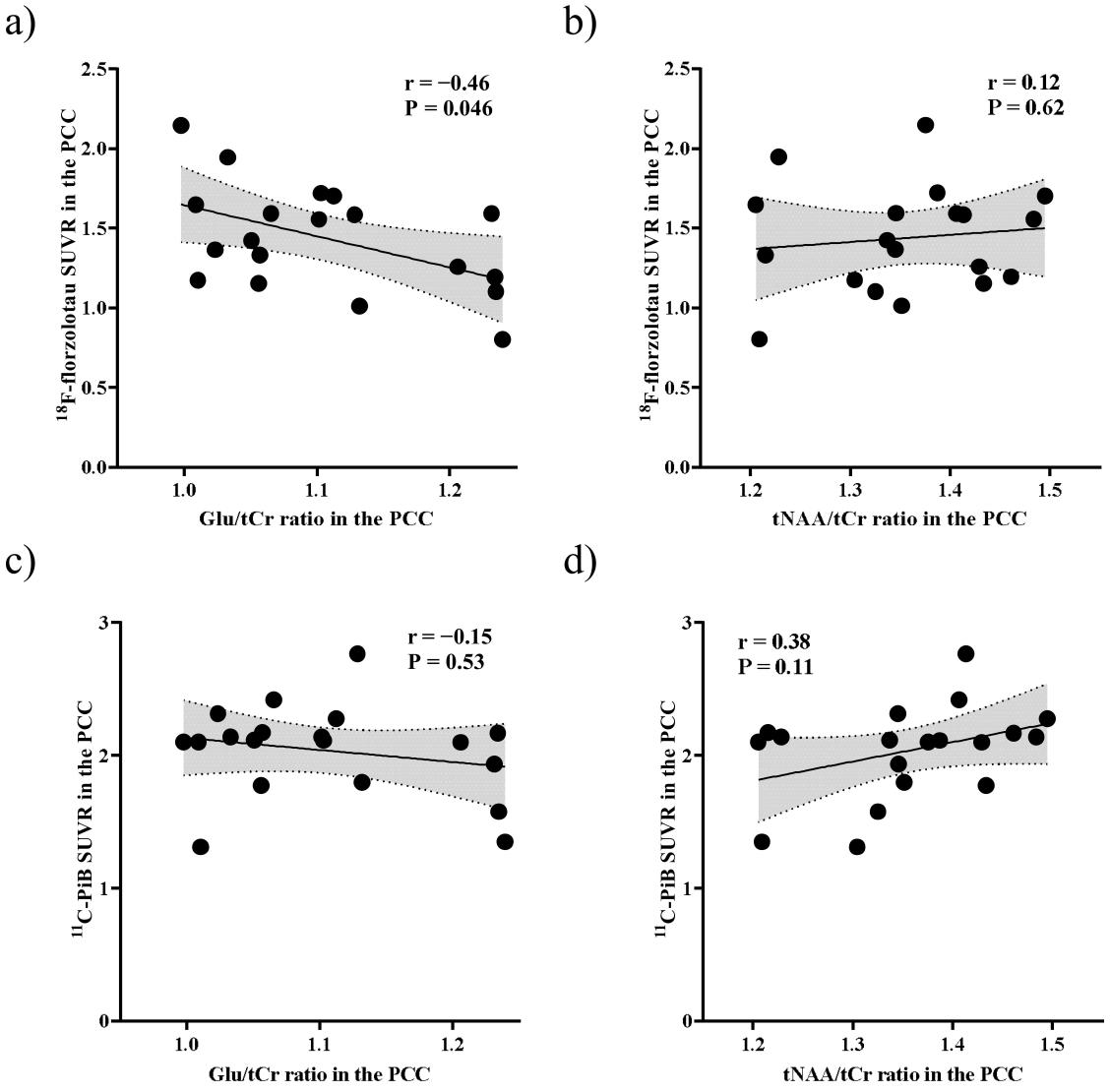
a)
r = −0.46
P = 0.046
18F-florzolotau SUVR in the PCC
Glu/tCr ratio in the PCC
b)
r = 0.12
P = 0.62
18F-florzolotau SUVR in the PCC
tNAA/tCr ratio in the PCC
c)
r = −0.15
P = 0.53
11C-PiB SUVR in the PCC
Glu/tCr ratio in the PCC
d)
r = 0.38
P = 0.11
11C-PiB SUVR in the PCC
tNAA/tCr ratio in the PCC

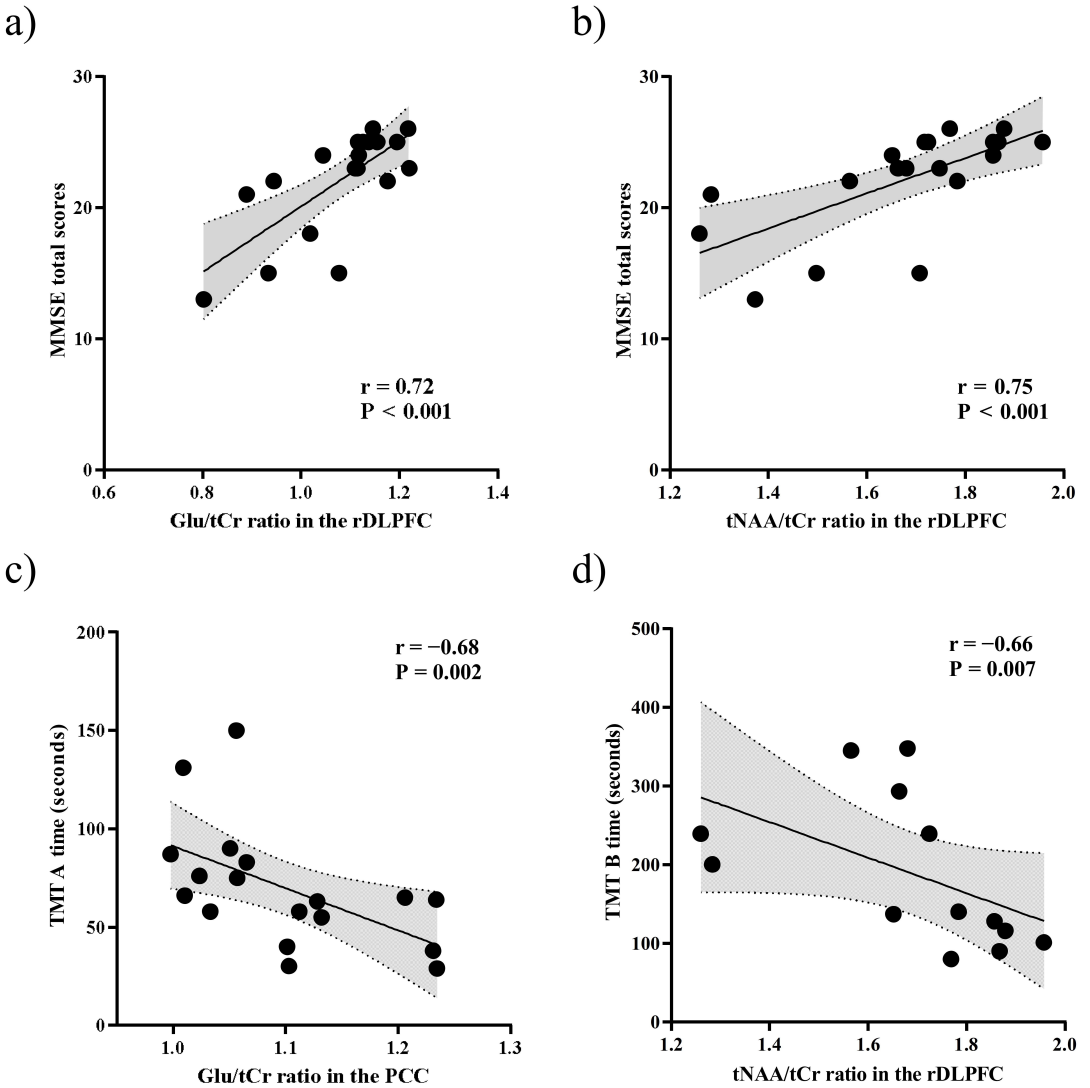
a)
MMSE total scores
Glu/tCr ratio in the rDLPFC
r = 0.72
P < 0.001
b)
MMSE total scores
tNAA/tCr ratio in the rDLPFC
r = 0.75
P < 0.001
c)
TMT A time (seconds)
Glu/tCr ratio in the PCC
r = −0.68
P = 0.002
d)
TMT B time (seconds)
tNAA/tCr ratio in the rDLPFC
r = −0.66
P = 0.007

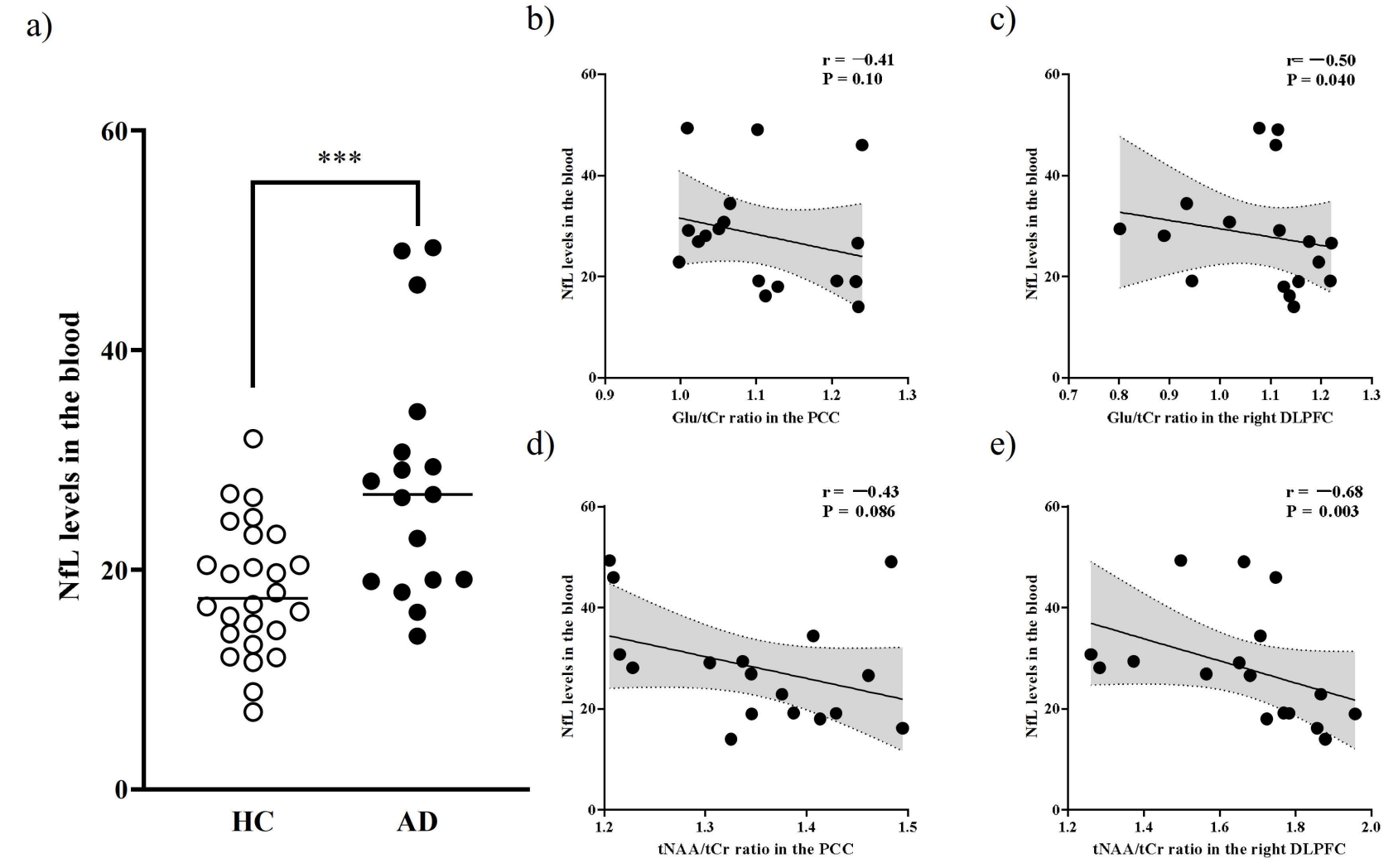
a)
***
NfL levels in the blood
60
40
20
0
HC
AD
b)
r = −0.41
P = 0.10
NfL levels in the blood
Glu/tCr ratio in the PCC
c)
r= −0.50
P = 0.040
NfL levels in the blood
Glu/tCr ratio in the right DLPFC
d)
r = −0.43
P = 0.086
NfL levels in the blood
tNAA/tCr ratio in the PCC
e)
r = −0.68
P = 0.003
NfL levels in the blood
tNAA/tCr ratio in the right DLPFC

Table 1. Demographic characteristics

	AD (n = 19)	HC (n = 26)		
	Mean (SD) or frequency (%)	Mean (SD) or frequency (%)	*t* or χ^2	P
Sex			$\chi^2 = 0.77$	0.28
Female	12 (63.2)	13 (50)		
Male	7 (36.8)	13 (50)		
Age, years	67.8 (9.4)	67.8 (7.5)	$t = -0.007$	0.99
Education, years	14.1 (1.9)	14.7 (1.5)	$t = -1.15$	0.26
MMSE	22.1 (4.0)	28.8 (1.3)	$t = -7.14$	<0.001
TMT-A time [a]	69.9 (31.5)	35.5 (9.2)	$t = 4.50$	<0.001
TMT-B time [b]	197.0 (93.6)	85.4 (32.0)	$t = 4.47$	<0.001
GDS	3.4 (2.2)	2.9 (2.8)	$t = 0.65$	0.52
Apathy Scale	13.5 (5.2)	10.9 (7.5)	$t = 1.32$	0.19
CDR global score		N/A	N/A	N/A
0.5	8 (42.1)			
1	9 (47.4)			
2	2 (10.5)			

Note: AD, Alzheimer's disease; CDR, clinical dementa rating; GDS, geriatric depression scale; HC, healthy control; MMSE, mini-mental state examination; SD, standard deviation; TMT, trail making test

[a] We presented available TMT-A data of 18 patients with AD/MCI and 26 HC participants.

[b] We presented available TMT-B data of 15 patients with AD/MCI and 26 HC participants.